ELSEVIER

International Journal of Solids and Structures 41 (2004) 859–870

INTERNATIONAL JOURNAL OF SOLIDS and STRUCTURES

www.elsevier.com/locate/ijsolstr

Postbuckling and vibration of a flexible strip clamped at its ends to a hinged substrate

Raymond H. Plaut [a,*], R. Paul Taylor [a], David A. Dillard [b]

[a] *Charles E. Via, Jr. Department of Civil and Environmental Engineering, Virginia Polytechnic Institute and State University, Blacksburg, VA 24061-0105, USA*

[b] *Department of Engineering Science and Mechanics, Virginia Polytechnic Institute and State University, Blacksburg, VA 24061-0219, USA*

Received 14 May 2003; received in revised form 16 September 2003

Abstract

A flexible strip is attached at its ends to a substrate comprised of two rigid plates connected with a hinge. One end of the strip is bonded to one of the plates, and the other end to the other plate. Initially the plates are flat and the strip has an upward (buckled) deflection. The right plate is rotated upward. This problem is motivated by an application of flexible electronic circuits in automobiles and possible debonding at the contact points with the substrate. The strip is modeled as an elastica. Equilibrium configurations and corresponding forces and moments are computed. If the system is symmetric, the strip contacts itself at a point when the rotation is sufficiently large. If the rotation is increased for an asymmetric system, the strip may jump to a shape having point contact with one of the plates and line contact with the other. Small vibrations about equilibrium are analyzed. The natural frequencies decrease as the rotation increases. Even though the strip is inextensible, the second mode has no nodes, and the number of extreme values in its shape increases as the rotation increases. Forced vibrations are also investigated, and the transmissibility is determined.

Keywords: Contact; Elastica; Equilibrium; Postbuckling; Shooting method; Vibrations

1. Introduction

Electronic circuits are often printed on flexible strips made of materials such as Mylar® or Kapton®. Known as flex circuits, these components find applications in many devices, including laptop computers and hinged electronic panels. In some applications, such as in automobiles, the strip may be bonded at two points to a substrate which is then folded to become a corner of a box. The strip is compressed and bulges outward, and there is a possibility of debonding due to high forces and moments. This problem is analyzed here.

* Corresponding author. Tel.: +1-540-231-6072; fax: +1-540-231-7532.
E-mail address: rplaut@vt.edu (R.H. Plaut).

0020-7683/$ - see front matter © 2003 Elsevier Ltd. All rights reserved.
doi:10.1016/j.ijsolstr.2003.09.057

The geometry is shown in Fig. 1 for the symmetric case. In Fig. 1(a), the two rigid plates comprising the substrate are horizontal. The strip is bonded to the substrate at its ends and has an initial deflection above it. The plates are assumed to continue past the bonded ends, which are represented by fixed supports in the analysis. The ends are at equal distances from the hinge connecting the plates. Then the right plate is rotated, and the configurations for rotations of $\pi/4$ and $\pi/2$ are sketched in Fig. 1(b) and (c), respectively. At a certain larger rotation, the two sides of the strip contact each other at a point (Fig. 1(d)), and if the rotation is increased further, the sides also touch the plates (Fig. 1(e) with dashed lines denoting the plates beyond the bonded ends of the strip).

A nonsymmetric case is depicted in Fig. 2, with the hinge closer to the right end of the strip than the left end. Rotations of $\pi/4$, $\pi/2$, and 2.36 are shown in Fig. 2(b)–(d), respectively. With further rotation, the strip may jump to a configuration as shown in Fig. 2(e), which contacts the left plate at a point and is flat along the upper plate near the clamped end. If the rotation is then increased to another threshold value, an internal point on the strip also contacts the second plate (Fig. 2(f)). If the rotation is decreased, the configuration of Fig. 2(e) is maintained until a certain rotation is reached, such as shown in Fig. 2(g), and then the strip jumps off the substrate into a shape with no contact.

The equilibrium problem is formulated in Section 2. The shape of the strip may involve no contact with the substrate (except at its ends), internal contact of the strip with itself at a point, and contact of the strip

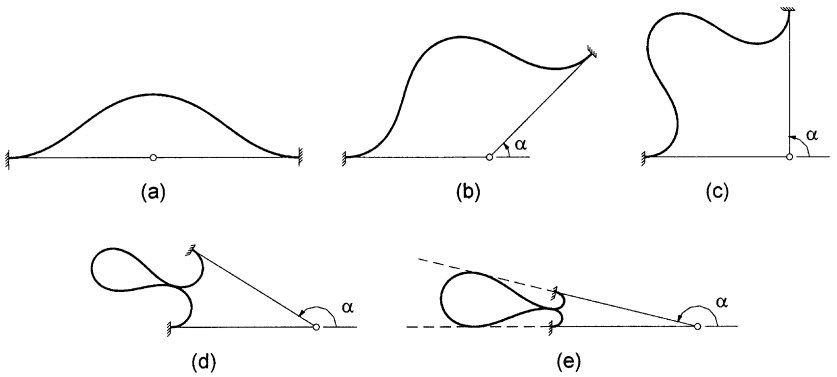

Fig. 1. Equilibrium shapes for symmetric case with $b = 0.45$ and rotation angle α equal to (a) 0, (b) $\pi/4$, (c) $\pi/2$, (d) 2.59, (e) 2.91 radians.

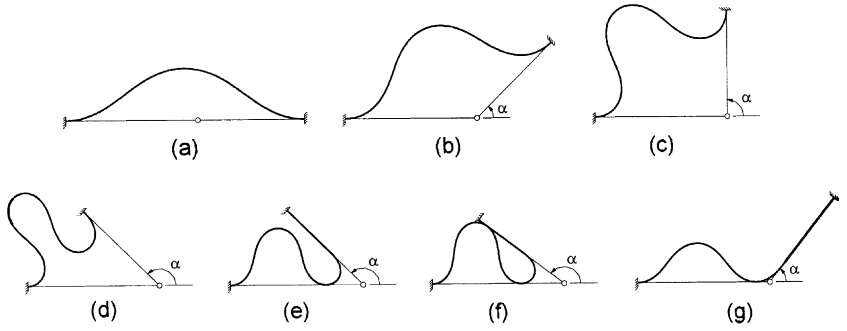

Fig. 2. Equilibrium shapes for asymmetric case with $b = 0.4$ and rotation angle α equal to (a) 0, (b) $\pi/4$, (c) $\pi/2$, (d) 2.36, (e) 2.37, (f) 2.50, (g) 0.903 radians.

with one plate at a point and with the other plate along a line. Numerical results for equilibrium of symmetric and asymmetric systems are presented in Section 3. In Section 4, free and forced vibrations are investigated. Motions about the equilibrium configuration are assumed to be small. Finally, concluding remarks are given in Section 5.

2. Formulation of equilibrium

Similar geometrical configurations arise in other types of problems. One is the blistering of liners inside cylindrical pipes, due to thermal differentials or external forces. Papers discussing this type of phenomenon include Li and Guice (1995), Boot and Welch (1996), Chunduru et al. (1996), Omara et al. (1997, 2000), Berti et al. (1999), Boot (1998), Boot and Naqvi (1998), El-Sawy and Moore (1998), Bakeer et al. (1999), Croll (2001), Dhar and Moore (2001), El-Sawy (2001, 2002), Thépot (2001), Zhao et al. (2001), and Zhu and Hall (2001). Another related problem is delamination of rings and shells due to bending or compressive loads. A few related references in this area are Kardomateas (1990, 1993, 1996), Kardomateas and Chung (1992), Kardomateas and Pelegri (1996), Yin (1996), El-Sayed and Srinivasan (2000), Rasheed and Tassoulas (2001, 2002), and Yu and Hutchinson (2002).

2.1. Cases with no contact

The substrate and strip are shown in a rotated configuration in Fig. 3, in nondimensional terms. The strip is assumed to be an elastica, which is thin, flexible, inextensible, unshearable, and unstrained when straight. It is uniform, with bending stiffness EI, and the bending moment is proportional to the curvature. Its ends are bonded to the substrate, and therefore fixed (clamped) boundary conditions are assumed. The substrate is comprised of two rigid plates hinged together along an axis on the plane of the substrate surface. The weight of the strip, and friction between the strip and the substrate, are neglected. In dimensional terms, the horizontal force is P, the vertical force is Q, the bending moment is M, the length of the strip is L, the length of the horizontal plate between the clamped end and the hinge is $L - B - \Delta$, the length of the rotating plate is B, the rotation angle of the right plate is α (measured in radians), the coordinates from the left end are X and Y, the arc length along the strip is S, and the rotation of the strip is θ. Since the length of the strip is greater than the length of the substrate, initially the strip exhibits a buckled shape.

The nondimensional quantities in Fig. 3 are defined as follows:

$$x = \frac{X}{L}, \quad y = \frac{Y}{L}, \quad s = \frac{S}{L}, \quad b = \frac{B}{L}, \quad \delta = \frac{\Delta}{L},$$

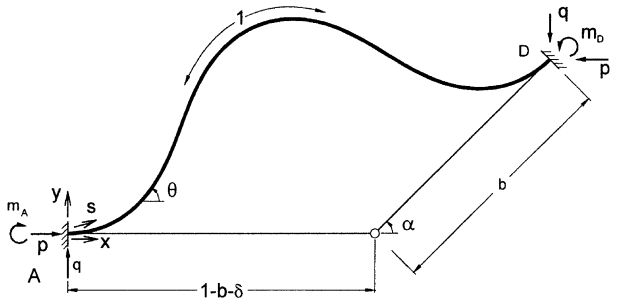

Fig. 3. Geometry in nondimensional terms when rotation angle is sufficiently small.

$$m = \frac{ML}{EI}, \quad p = \frac{PL^2}{EI}, \quad q = \frac{QL^2}{EI} \tag{1}$$

Subscripts A and D on m denote the ends of the strip. The governing equations, based on geometry, moment–curvature relation, and equilibrium of an element, are

$$\frac{dx}{ds} = \cos\theta, \quad \frac{dy}{ds} = \sin\theta, \quad \frac{d\theta}{ds} = m, \quad \frac{dm}{ds} = q\cos\theta - p\sin\theta \tag{2}$$

The boundary conditions at $s = 0$ are $x = y = \theta = 0$ and $m = m_A$. At $s = 1$, they are $x = 1 - b - \delta + b\cos\alpha$, $y = b\sin\alpha$, $\theta = \alpha$, and $m = m_D$. Numerical solutions are obtained in this study using a shooting method in Mathematica (Wolfram, 1991).

For cases such as those in Figs. 1(a)–(c) and 2(a)–(d), in which the strip is free between its ends (i.e., no self-contact or contact with the substrate), Eqs. (2) are solved. The quantities b, δ, and α are specified, and the quantities p, q, and m_A are varied until numerical integration of Eqs. (2) leads to satisfaction of the first three boundary conditions at $s = 1$ with sufficient accuracy.

2.2. Symmetric case with self-contact

In the case of symmetry in Fig. 1(a), i.e., if $b = (1 - \delta)/2$, self-contact can occur at a point, as shown in Fig. 4. Similar loops have been analyzed in several papers, including Flaherty and Keller (1973), Wang (1981), Bottega (1991), and Plaut et al. (1999). Here B denotes the contact point and C denotes the furthest point on the loop from the hinge along the line connecting B and the hinge (which has angle $(\pi - \alpha)/2$ with each plate). The resultant nondimensional reaction force at A and D is denoted r and is oriented along the line connecting A and D (which has angle $\alpha/2$ with the horizontal), so that $p = r\cos(\alpha/2)$ and $q = r\sin(\alpha/2)$ in Eqs. (2). (For the symmetric case, these relationships also can be used when there is no contact.)

The resultant force in the loop BC is denoted r_{BC}. It is constant and acts parallel to the vectors r in Fig. 4, directed upward in the lower branch of the loop and downward in the upper branch. The value of the bending moment in each branch of the loop at the contact point B is denoted m_B, and the bending moment at C is m_C. Using results in Wang (1981), one can show that

$$(0.5 - d)m_B = 3.027634, \quad m_B = 0.96163\sqrt{r_{BC}}, \quad m_C = -1.71018\sqrt{r_{BC}} \tag{3}$$

From geometry, $y\tan(\alpha/2) = b - x$ at B and C, $\theta = (\pi + \alpha)/2$ at B, and $\theta = \alpha/2$ at C. The section from A to B has unknown length d. The quantities b and α are specified. Eqs. (2), with the last one replaced by

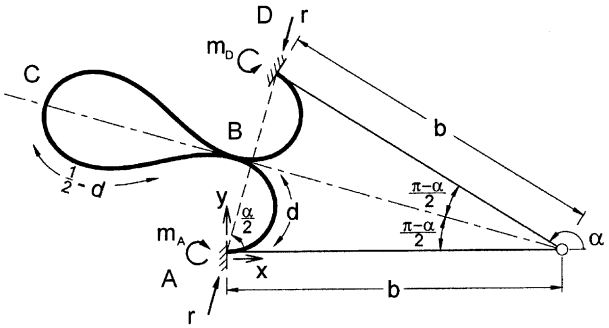

Fig. 4. Geometry for symmetric case when self-contact occurs.

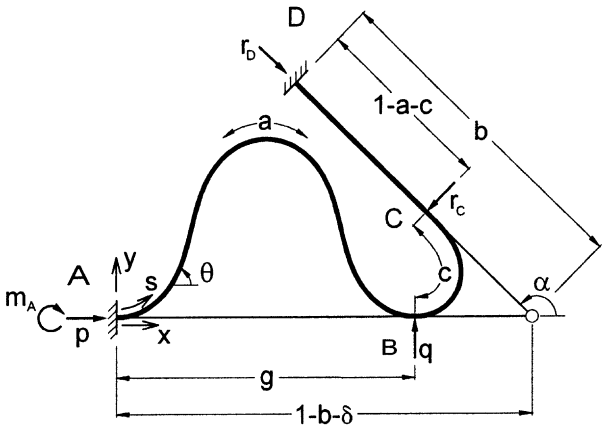

Fig. 5. Geometry for asymmetric case when strip contacts (longer) bottom plate.

$dm/ds = r\sin[(\alpha/2) - \theta]$, are integrated from A to B and from B to C (with r replaced by r_{BC} between B and C). The quantities r, d, and m_A are varied until the known conditions at B and C are satisfied.

If the rotation angle α increases until a point in section BC touches the horizontal plate, as occurs in Fig. 1(e) for the extended horizontal plate, this analysis becomes invalid.

2.3. Asymmetric case with contact of strip and substrate

If the hinge is not equally spaced from the fixed ends A and C, the configuration shown in Fig. 5 may occur. The section from A to B is the same as a buckled elastica with clamped ends, and has no shear force. It is convenient to make use of the solution for that section in terms of elliptic integrals (Timoshenko and Gere, 1961, Plaut et al., 1999):

$$g = 4[2E(k) - K(k)]/\sqrt{p}, \quad a = 4K(k)/\sqrt{p}, \quad m_A = m_B = 2k\sqrt{p} \tag{4}$$

where g is the value of x at B, a is the arc length from A to B, $E(k)$ and $K(k)$ are complete elliptic integrals of the first and second kind, respectively, and $0 < k < 1$. The associated shape of the strip can be obtained by solving Eqs. (2) with $q = 0$.

The shooting method is used with Eqs. (2) from B to C, where p is the same as in section AB since friction is neglected. The quantities p, q, k, and c (arc length from B to C) are treated as unknowns, and Eqs. (4) give g, a, and m_B in terms of them. At C, the values of x and y can be deduced from Fig. 5, $\theta = \alpha$, and $m_C = 0$ (since section CD has no curvature or moment). In the result, q must be nonnegative for this configuration to be possible.

At a threshold value of α, the rotating plate makes contact with section AB, as shown in Fig. 2(f), and this analysis becomes invalid for higher values of α.

3. Equilibrium results

3.1. Symmetric case

Numerical results are presented first for the symmetric case with $b = 0.49$ (i.e., $\delta = 0.02$), $b = 0.45$ ($\delta = 0.10$), and $b = 0.40$ ($\delta = 0.20$). Some configurations when $b = 0.45$ are depicted in Fig. 1. As the

rotation angle α is increased from $\alpha = 0$ for this case, self-contact occurs first when $\alpha = 2.59$ (Fig. 1(d)), and contact with the plates is exhibited when α reaches 2.91 (Fig. 1(e)). Results were not computed for $\alpha > 2.91$. The corresponding values of α for self-contact and plate contact when $b = 0.49$ are 2.63 and 2.92, respectively, and when $b = 0.40$ they are 2.52 and 2.88.

Fig. 6(a) shows how the equal bending moments at the ends of the strip increase as α increases. For $b = 0.49$, the moments are equal to 1.78 at $\alpha = 0$, 7.28 at $\alpha = \pi/2$, 12.2 at $\alpha = 2.63$, and 16.0 at $\alpha = 2.92$. For $b = 0.45$, they are 4.05 at $\alpha = 0$, 8.31 at $\alpha = \pi/2$, 12.3 at $\alpha = 2.59$, and 16.7 at $\alpha = 2.91$. On the upper curve, they are 5.85 at $\alpha = 0$, 9.47 at $\alpha = \pi/2$, 12.6 at $\alpha = 2.52$, and 17.7 at $\alpha = 2.88$.

The horizontal and vertical components of the forces in the strip are plotted in Fig. 6(b) for $b = 0.45$. For $0 < \alpha < 2.59$, these forces are constant along the entire strip. At $\alpha = 0$, $\pi/2$, 2.59, and 2.91, respectively, the values of p are 41.6, 50.3, 28.5, and 112, and the values of q are 0, 50.3, 99.6, and 941. The curves for $b = 0.49$ and 0.40 are not plotted. For $b = 0.49$, the values of p at $\alpha = 0$, $\pi/2$, 2.63, and 2.92, respectively, are 39.9, 50.2, 26.3, and 99.4, and the values of q are 0, 50.2, 101, and 885. For $b = 0.40$, the values of p at $\alpha = 0$, $\pi/2$, 2.52, and 2.88, respectively, are 43.9, 51.2, 31.5, and 130, and the values of q are 0, 51.2, 97.6, and 1,010.

For $2.59 < \alpha < 2.91$, the forces plotted in Fig. 6(b) are those for the sections from the fixed ends to the point of self-contact, including the reaction forces. The vertical force component, q, becomes very large in this region, and the horizontal force component, p, also increases significantly. The reactions at the bonded ends of the strip are equal to the moments and forces shown in Fig. 6, and can be used to help determine whether a given strip will remain in equilibrium, or whether the strength of the bonding will be insufficient and debonding will occur.

3.2. Asymmetric case

The case of $b = 0.4$ and $\delta = 0.1$ was analyzed in detail. The stationary horizontal plate has non-dimensional length 0.5. Some equilibrium shapes for this case are presented in Fig. 2.

The end moments are plotted in Fig. 7(a). When the right plate is horizontal, these moments are both equal to 4.05. As the plate is rotated, the moments increase, with $m_A > m_D$. At $\alpha = \pi/2$, $m_A = 9.06$ and $m_D = 7.17$. At $\alpha = 2.36$, where $m_A = 14.8$ and $m_D = 3.32$, the curves exhibit a vertical tangent. The equilibrium shape with no internal contact (Fig. 2(e)) becomes unstable, and the strip jumps to a state as shown in Fig. 2(f). The moment m_D becomes zero and the moment m_A jumps to the value 14.4 on the other solid

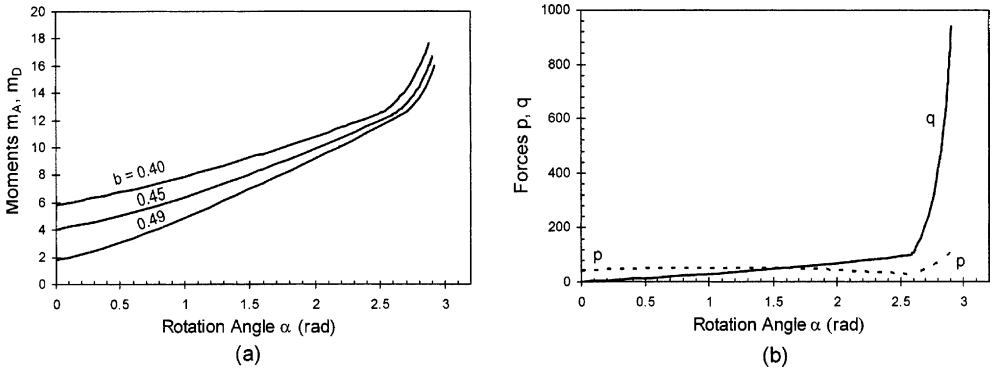

Fig. 6. Symmetric case, influence of rotation on: (a) end moments with $b = 0.49$ ($\delta = 0.02$), $b = 0.45$ ($\delta = 0.10$), $b = 0.40$ ($\delta = 0.20$); (b) forces with $b = 0.45$ ($\delta = 0.10$).

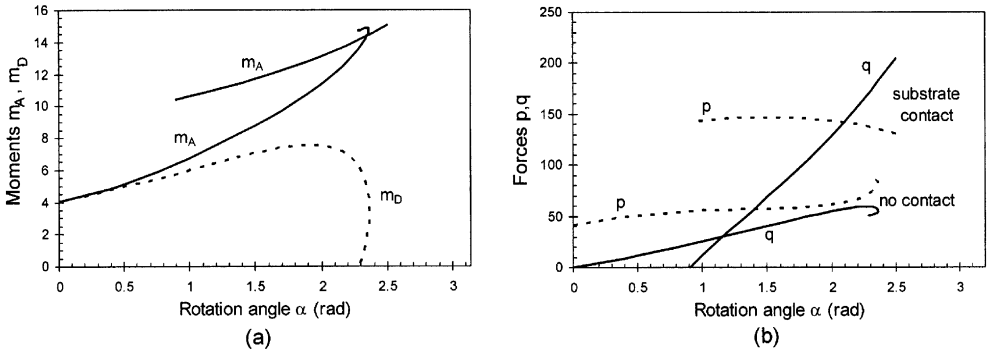

Fig. 7. Asymmetric case with $b = 0.4$ and $\delta = 0.1$, influence of rotation on: (a) end moments; (b) forces.

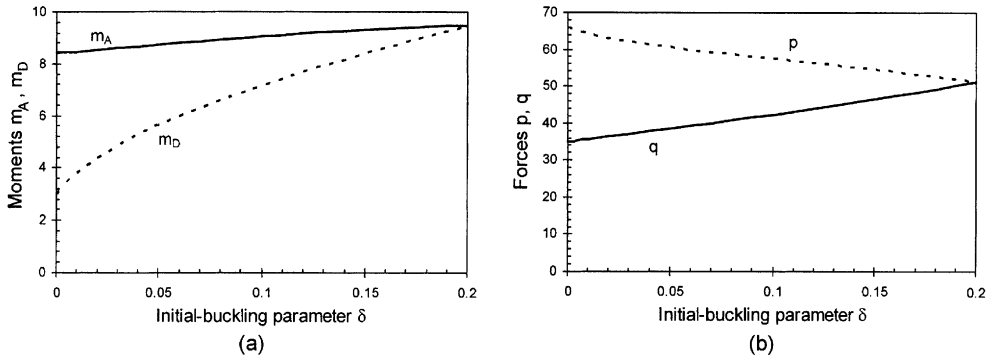

Fig. 8. Asymmetric case, $b = 0.4$ and $\alpha = \pi/2$, influence of amount of initial buckling on: (a) end moments; (b) forces.

curve in Fig. 7(a). If α is increased further, m_A increases till the strip contacts the horizontal plate (when α reaches 2.50), as shown in Fig. 2(f). Higher values of α were not considered.

If the right plate is rotated past $\alpha = 2.36$ and then is rotated back towards $\alpha = 0$ (i.e., clockwise), the strip remains in a shape like that in Fig. 2(e) until α is reduced to 0.903 (shown in Fig. 2(g)). At that time, the reaction force q at B in Fig. 5 becomes zero, and the strip snaps into a shape having no contact with the substrate. In Fig. 7(a), m_A jumps from the left end of the upper curve (where $m_A = 10.4$) to the lower solid curve (where $m_A = 6.35$), and m_B jumps from zero to the value 5.79 on the dashed curve at that rotation angle.

The forces in the strip are plotted in Fig. 7(b). They increase as α increases except for q when the vertical tangent in the figure is approached. At $\alpha = 0$, $\pi/2$, and 2.36, respectively, the values of p are 41.6, 57.6, and 83.7, and the values of q are 0, 42.3, and 54.7. As α passes 2.36, p jumps to 136 and q jumps to 183. If α is increased further, p decreases and q increases until the configuration in Fig. 2(f) occurs at $\alpha = 2.50$ with $p = 131$ and $q = 204$. If α is decreased, p increases and then decreases to 143, while q decreases steadily till it reaches zero, at which point the strip jumps to a no-contact shape with $p = 54.8$ and $q = 27.3$.

Results before internal contact occurs were also obtained for other cases, such as $b = 0.3$ and $\delta = 0.1$ (in which the stationary plate is twice as long as the rotating plate). The forms of the moment and force curves are similar to those in Fig. 7.

For asymmetric cases with $b = 0.4$ and $\alpha = \pi/2$ (i.e., the rotating plate is vertical), the effect of the amount of initial buckling is depicted in Fig. 8, where δ ranges from 0 to 0.2 (a symmetric case). As δ increases, the end moments increase, p decreases, and q increases.

4. Small vibrations about equilibrium

First, free vibrations of the strip about its equilibrium configuration are analyzed for cases of no contact (as in Fig. 3). The nondimensional frequency and time are denoted ω and t, respectively. In terms of dimensional time T and frequency Ω,

$$\omega = \Omega L^2 \sqrt{\frac{\mu}{EI}}, \quad t = \frac{T}{L^2}\sqrt{\frac{EI}{\mu}} \tag{5}$$

where μ is the mass per unit length of the strip. In nondimensional terms, the governing equations are given by Eqs. (2), with ordinary derivatives replaced by partial derivatives, together with

$$\frac{\partial p}{\partial s} = -\frac{\partial^2 x}{\partial t^2}, \quad \frac{\partial q}{\partial s} = -\frac{\partial^2 y}{\partial t^2} \tag{6}$$

The force components $p(s,t)$ and $q(s,t)$ are not constant along the strip during motion.

Equilibrium values are denoted with a subscript "e" and mode shapes with a subscript "d" signifying "dynamic." For vibrations at frequency ω, the variables are written in the form

$$x(s,t) = x_e(s) + x_d(s)\sin\omega t, \quad y(s,t) = y_e(s) + y_d(s)\sin\omega t, \quad \theta(s,t) = \theta_e(s) + \theta_d(s)\sin\omega t,$$

$$m(s,t) = m_e(s) + m_d(s)\sin\omega t, \quad p(s,t) = p_e + p_d(s)\sin\omega t, \quad q(s,t) = q_e + q_d(s)\sin\omega t \tag{7}$$

These expressions are used in Eqs. (2) and (6), then the equilibrium equations are utilized to eliminate some terms, and finally the equations in the dynamic variables are linearized. This leads to the governing equations

$$\frac{dx_d}{ds} = -\theta_d \sin\theta_e \quad \frac{dy_d}{ds} = \theta_d \cos\theta_e, \quad \frac{d\theta_d}{ds} = m_d,$$

$$\frac{dm_d}{ds} = (q_d - p_e\theta_d)\cos\theta_e - (p_d + q_e\theta_d)\sin\theta_e,$$

$$\frac{dp_d}{ds} = \omega^2 x_d, \quad \frac{dq_d}{ds} = \omega^2 y_d \tag{8}$$

At $s = 0$ and $s = 1$, the boundary conditions on the dynamic variables are $x_d = y_d = \theta_d = 0$.

A shooting method is used to obtain the natural frequencies and modes. Since the modal amplitude is arbitrary, $m_d(0)$ is specified (for example), and $p_d(0)$, $q_d(0)$, and ω are varied until the boundary conditions at $s = 1$ are satisfied, with initial guesses for ω chosen in different ranges to obtain several of the lowest frequencies and corresponding modes.

Results are presented for the symmetric case with $b = 0.45$ (and hence $\delta = 0.1$). Fig. 9 shows how the lowest three nondimensional natural frequencies vary with the rotation angle α, with $0 < \alpha < \pi/2$. The frequencies decrease as α increases in this range (i.e., as the right plate is raised from a horizontal position to a vertical position). At $\alpha = 0$, these frequencies are $\omega = 43.9$, 75.8, and 153.0, while the first three natural frequencies for $\alpha = \pi/2$ are $\omega = 39.3$, 49.9, and 66.1.

Fig. 10 shows the first three modes when $\alpha = 0$, and Fig. 11 depicts these modes when $\alpha = \pi/2$. The shapes represent the normal displacement of the strip. The first and third modes are anti-symmetric about the center of the strip, while the second mode is symmetric. Due to inextensibility of the strip, the mode shape must have the same length as the strip. Therefore it may seem surprising that the second mode has no nodes. This is possible because the equilibrium configuration has two inflection points. If the strip is vibrating in the second mode and is above the equilibrium shape, the portions of the mode near the ends are shorter than the corresponding portions of the equilibrium shape, which can make up for the longer portion in the middle where the mode passes over the hump. It is also interesting that the second mode has two local

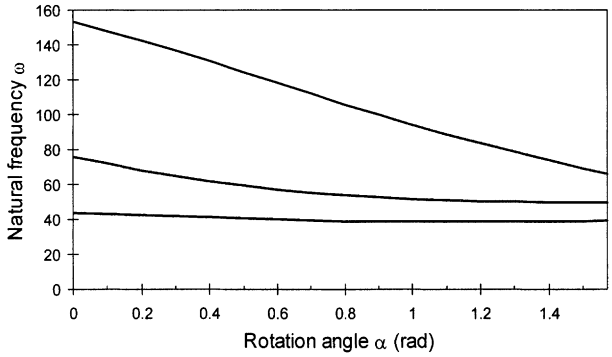

Fig. 9. Influence of rotation on lowest three natural frequencies.

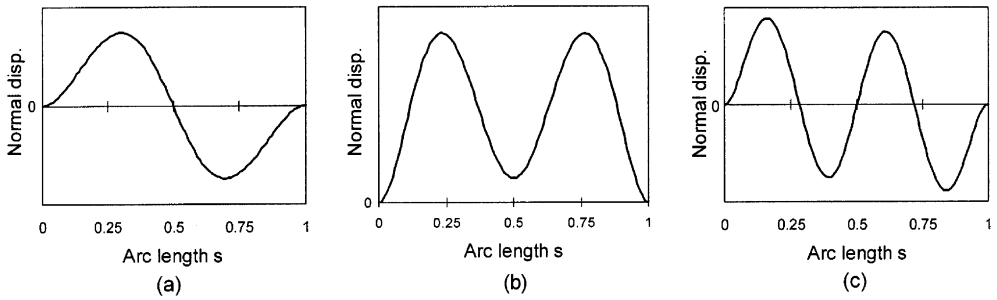

Fig. 10. First three mode shapes when $b = 0.45$ ($\delta = 0.1$) and $\alpha = 0$.

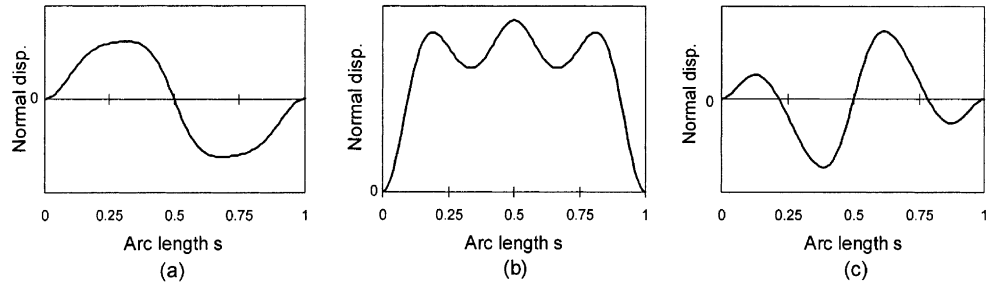

Fig. 11. First three mode shapes when $b = 0.45$ ($\delta = 0.1$) and $\alpha = \pi/2$.

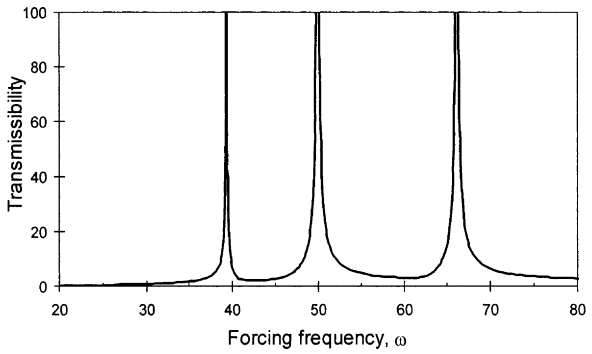

Fig. 12. Influence of forcing frequency on transmissibility when $b = 0.45$ ($\delta = 0.1$) and $\alpha = \pi/2$.

maxima in Fig. 10(b) and three local maxima in Fig. 11(b). The transition between these two configurations occurs when α is approximately 1.2.

Now forced vibrations are considered. The case $\alpha = \pi/2$ is analyzed, with $b = 0.45$ and $\delta = 0.1$ again. The horizontal plate is given a small, harmonic, vertical motion $y_0 \sin \omega t$, related to the application of a flexible electronic circuit in a corner of a box and in a moving automobile. A term $\omega^2 y_0$ is added to the right side of the last equation in Eqs. (8). The forcing frequency ω is specified, and the quantity m_d (0) replaces ω as an unknown in the shooting method previously used for free vibrations.

The displacement transmissibility is defined here as the absolute value of the ratio $y_d(0.5)/y_0$, where the numerator is the amplitude of the vertical motion (from equilibrium) at the center of the strip. The transmissibility is plotted in Fig. 12 as a function of the nondimensional forcing frequency ω for the range $20 < \omega < 80$. Damping has not been included in the analysis. The spikes are associated with the natural frequencies of free vibration for this case.

5. Concluding remarks

Postbuckling and vibrations of an elastica have been investigated. The ends of the strip were fixed to a hinged substrate, and the strip had some initial deflection when the two plates comprising the substrate were horizontal. One side was then rotated, causing the strip to fold into a postbuckled shape. For a symmetric system, two sides of the strip contact each other at a certain rotation, and continue to exhibit point contact for further rotation. For an asymmetric system, after further rotation the strip may snap into a configuration with point contact along the longer plate and line contact (adjacent to the fixed end) along the shorter plate. If the rotation is then reduced, the strip remains in this shape until a threshold rotation angle is reached, and then snaps to a shape having no internal contact with the substrate.

Small free and forced vibrations were analyzed. The lowest natural frequency corresponds to an antisymmetric mode. The second mode is symmetric and has no nodes, which is unusual for an inextensible strip. For the numerical example presented here, the number of local extreme points in the second mode changes as the rotation changes. As usual, the dynamic response to a harmonic excitation can become large when the forcing frequency is near one of the natural frequencies.

This analysis was motivated by an application of flexible electronic circuits in automobiles. It also is related to problems of buckling of liners inside cylinders, and delamination of composite materials. Debonding is sometimes predicted with the use of a critical value of the energy release rate G. At the bonded ends of the strip, the effect of the forces on G is negligible compared to the effect of the bending moment,

and G is approximately given by $M^2/(2EIW)$ where W is the width of the strip (Suo and Hutchinson, 1990, Papini and Spelt, 2002). The bending moment M can be obtained from results such as shown in Figs. 6(a) and 7(a), which can then be used to predict whether or not debonding will occur.

Acknowledgements

This research was supported by a scholarship to Paul Taylor from the Adhesive and Sealant Council Educational Foundation (ASCEF) and from the Center for Adhesive and Sealant Science (CASS) at Virginia Tech. The authors are grateful to the reviewers for their helpful comments.

References

Bakeer, R.M., Barber, M.E., Pechon, S.E., Taylor, J.E., Chunduru, S., 1999. Buckling of HDPE liners under external uniform pressure. Journal of Materials in Civil Engineering 11 (4), 353–361.

Berti, D., Stutzman, R., Lindquist, E., Eshghipour, M., 1999. Buckling of steel tunnel liner under external pressure. Journal of Energy Engineering 124 (3), 55–89.

Boot, J.C., 1998. Elastic buckling of cylindrical pipe linings with small imperfections subject to internal pressure. Trenchless Technology Research 12 (1), 3–15.

Boot, J.C., Naqvi, M.M., 1998. Structural considerations for thermoplastic pipe linings used for transport of aggressive hydrocarbons. Plastics, Rubber and Composites Processing and Applications 27 (9), 424–429.

Boot, J.C., Welch, A.J., 1996. Creep buckling of thin-walled polymeric pipe linings subject to external groundwater pressure. Thin-Walled Structures 24 (3), 191–210.

Bottega, W.J., 1991. Peeling and bond-point propagation in a self-adhered elastica. Quarterly Journal of Mechanics and Applied Mathematics 44 (1), 17–33.

Chunduru, S., Barber, M.E., Bakeer, R.M., 1996. Buckling behavior of polyethylene liner system. Journal of Materials in Civil Engineering 8 (4), 201–206.

Croll, J.A., 2001. Buckling of cylindrical tunnel liners. Journal of Engineering Mechanics 127 (4), 333–341.

Dhar, A.S., Moore, I.D., 2001. Liner buckling in profiled polyethylene pipes. Geosynthetics International 8 (4), 303–326.

El-Sawy, K.M., 2001. Inelastic stability of tightly fitted cylindrical liners subjected to external uniform pressure. Thin-Walled Structures 39 (9), 731–744.

El-Sawy, K.M., 2002. Inelastic instability of loosely fitted cylindrical liners. Journal of Structural Engineering 128 (7), 934–941.

El-Sawy, K., Moore, I.D., 1998. Stability of loosely fitted liners used to rehabilitate rigid pipes. Journal of Structural Engineering 124 (11), 1350–1357.

El-Sayed, S., Srinivasan, S., 2000. Delamination buckling and growth in rings under pressure. Journal of Engineering Mechanics 126 (10), 1033–1039.

Flaherty, J.E., Keller, J.B., 1973. Contact problems involving a buckled elastica. SIAM Journal on Applied Mathematics 24 (2), 215–225.

Kardomateas, G.A., 1990. Snap buckling of delaminated composites under pure bending. Composites Science and Technology 39 (1), 63–74.

Kardomateas, G.A., 1993. The initial post-buckling and growth behavior of internal delaminations in composite plates. Journal of Applied Mechanics 60 (4), 903–910.

Kardomateas, G.A., 1996. Predicting the growth of internal delaminations under monotonic or cyclic compression. Key Engineering Materials 121/122, 441–462.

Kardomateas, G.A., Chung, C.B., 1992. Thin film modeling of delamination buckling in pressure loaded laminated cylindrical shells. AIAA Journal 30 (8), 2119–2123.

Kardomateas, G.A., Pelegri, A.A., 1996. Growth behavior of internal delaminations in composite beam/plates under compression: Effect of the end conditions. International Journal of Fracture 75 (1), 49–67.

Li, J.Y., Guice, L.K., 1995. Buckling of encased elliptic thin ring. Journal of Engineering Mechanics 121 (12), 1325–1329.

Omara, A.M., Guice, L.K., Straughan, W.T., Akl, F., 1997. Buckling models of thin circular pipes encased in rigid cavity. Journal of Engineering Mechanics 123 (12), 1294–1301.

Omara, A.M., Guice, L.K., Straughan, W.T., Akl, F., 2000. Instability of thin pipes encased in oval rigid cavity. Journal of Engineering Mechanics 126 (4), 381–388.

Papini, M., Spelt, J.K., 2002. The mechanics of coatings, in: Dillard, D.A., Pocius, A.V. (Eds.), The Mechanics of Adhesion. Elsevier, Amsterdam, pp. 303–350.

Plaut, R.H., Suherman, S., Dillard, D.A., Williams, B.E., Watson, L.T., 1999. Deflections and buckling of a bent elastica in contact with a flat surface. International Journal of Solids and Structures 36 (8), 1209–1229.

Rasheed, H.A., Tassoulas, J.L., 2001. Delamination growth in long composite tubes under external pressure. International Journal of Fracture 108 (1), 1–23.

Rasheed, H.A., Tassoulas, J.L., 2002. Collapse of composite rings due to delamination buckling under external pressure. Journal of Engineering Mechanics 128 (11), 1174–1181.

Suo, Z., Hutchinson, J.W., 1990. Interface crack between two elastic layers. International Journal of Fracture 43 (1), 1–18.

Thépot, O., 2001. Structural design of oval-shaped sewer linings. Thin-Walled Structures 39 (6), 499–518.

Wang, C.-Y., 1981. Folding of elastica—similarity solutions. Journal of Applied Mechanics 48 (1), 199–200.

Wolfram, S., 1991. Mathematica: A System for Doing Mathematics by Computer. Addison-Wesley, Reading, MA.

Yin, W.L., 1996. Snap buckling of thin delaminated layers in a contracting cylinder. Key Engineering Materials 120, 427–439.

Yu, H.H., Hutchinson, J.W., 2002. Influence of substrate compliance on buckling of thin films. International Journal of Fracture 113 (1), 39–55.

Zhao, Q.G., Nassar, R., Hall, D.E., 2001. Numerical simulation of creep-induced buckling of thin-walled pipe liners. Journal of Pressure Vessel Technology 123 (3), 373–380.

Zhu, M., Hall, D.E., 2001. Creep induced contact and stress evolution in thin-walled pipe liners. Thin-Walled Structures 39 (11), 939–959.